

Yuan Shi, Fabia Süß, Jürgen Horvath, Dietmar Koch, Kamen Tushtev

Evaluation of mechanical properties of a dense SiC/SiCN composite  
produced via PIP process

Journal Article as: peer-reviewed accepted version (Postprint)

DOI of this document\* (secondary publication): 10.26092/elib/2918

Publication date of this document: 11/04/2024

\* for better findability or for reliable citation

**Recommended Citation (primary publication/Version of Record) incl. DOI:**

Yuan Shi , Fabia Süß, Jürgen Horvath, Dietmar Koch, Kamen Tushtev: Evaluation of mechanical properties of a  
dense SiC/SiCN composite produced via PIP process  
Journal of the European Ceramic Society, Volume 42, Issue 3, 2022, Pages 775-785  
ISSN 0955-2219  
<https://doi.org/10.1016/j.jeurceramsoc.2021.11.009>

Please note that the version of this document may differ from the final published version (Version of Record/primary  
publication) in terms of copy-editing, pagination, publication date and DOI. Please cite the version that you actually used.  
Before citing, you are also advised to check the publisher's website for any subsequent corrections or retractions  
(see also <https://retractionwatch.com/>).

This document is made available with all rights reserved.

The license information is available online: <https://creativecommons.org/licenses/by-nc-nd/4.0/>

**Take down policy**

If you believe that this document or any material on this site infringes copyright, please contact  
[publizieren@suub.uni-bremen.de](mailto:publizieren@suub.uni-bremen.de) with full details and we will remove access to the material.

# Evaluation of mechanical properties of a dense SiC/SiCN composite produced via PIP process

Yuan Shi <sup>a,\*</sup>, Fabia Süß <sup>a,1</sup>, Jürgen Horvath <sup>b</sup>, Dietmar Koch <sup>c</sup>, Kamen Tushtev <sup>b</sup>

<sup>a</sup> Institute of Structures and Design, German Aerospace Center Stuttgart, Pfaffenwaldring 38-40, 70569, Stuttgart, Germany

<sup>b</sup> Advanced Ceramics, University of Bremen, Am Biologischen Garten 2, 28359, Bremen, Germany

<sup>c</sup> Institute of Materials Resource Management, University of Augsburg, Am Technologiezentrum 8, 86159, Augsburg, Germany

## ARTICLE INFO

### Keywords:

Ceramic-matrix composites (CMCs)  
SiC/SiCN  
Mechanical behavior  
Weak Matrix Composites (WMC) and Weak Interface Composites (WIC)  
High-temperature properties

## ABSTRACT

The material behavior of Polymer Infiltration and Pyrolysis based SiC/SiCN composites is studied and the characteristic thermal and mechanical properties in on- (0/90 °) and off-axis ( $\pm 45^\circ$ ) direction are summarized. The tensile properties are determined at room temperature and 1300 °C. Based on the ratio of Young's modulus and strength between on- and off-axis loading, a new approach for the classification of Weak Matrix Composites (WMC) and Weak Interface Composites (WIC) is proposed, which seems to be reasonable for various CMCs. Even without fibre coating mechanical behavior of SiC/SiCN is similar to that of WIC. In order to explain this, a microstructure model is developed and confirmed by analysis of fracture surface. The effect of temperature on the tensile properties is investigated through analysis of residual thermal stresses. Even though at 1300 °C the strength is slightly lower, the fracture strain increased significantly from RT to 1300 °C.

## 1. Introduction and objective

SiC fibre reinforced silicon carbide (SiC/SiC) is a promising composite material for use in high temperature structural applications, e.g., as components in gas turbines. In contrast to superalloys SiC/SiC composites show lower density and higher temperature capability. Their use in gas turbine engines leads to weight reduction, higher fuel efficiency and reduced emission [1,2]. There are several fabrication routes to manufacture SiC matrices which influence the resulting material properties and mechanical behavior. The most important routes are chemical vapor infiltration (CVI), (reactive) melt infiltration (R)MI, and polymer infiltration and pyrolysis (PIP) [3]. The characteristic features of the processes and resulting materials are described in the following section.

CVI SiC/SiC composites have a nearly stoichiometric SiC matrix with high strength and stiffness and a residual open porosity of 10–15 %. The SiC matrix is deposited from the gas phase. For damage tolerant fracture behavior, a weak interphase (e.g., boron nitride - BN or pyrolytic carbon - pyC) has to be introduced prior to matrix infiltration [3–5].

In contrast, the (R)MI process yields SiC/SiC composites with a dense matrix (open porosity below 3 %). Due to the manufacturing process, the composites show a residual silicon content of up to 15 %. The silicon melt infiltrates a porous carbon structure forced by capillary effects. The

melt reacts with the porous carbon forming the SiC matrix [6,7]. Similar to the CVI route, the (R)MI route also introduces a weak interphase in the form of pyC or BN to achieve damage tolerant fracture behavior [3, 7–9].

In the PIP manufacturing, which is also used for the material tested in this work, a low viscous preceramic precursor is infiltrated into a fibre preform. After curing, the SiC fibre reinforced polymer is pyrolyzed in inert gas atmosphere at elevated temperatures of about 900 °C–1300 °C. The preceramic precursor then converts into a ceramic matrix, mostly SiC, SiCO or SiCN. Due to the shrinkage of the polymer, a high amount of porosity is formed. Therefore, up to 10 cycles of infiltration and pyrolysis are usually needed to reduce the remaining porosity to about 5 %. In contrast to (R)MI route, there is no residual silicon present in the matrix. A pyC interphase may be applied prior first polymer infiltration, but is not mandatory for good damage tolerance [3,10,11]. Furthermore, PIP process can be easily combined with other manufacturing techniques. In literature are described for example CVI manufacturing followed by PIP process [9] or PIP manufacturing followed by a final liquid silicon infiltration (LSI) step [12].

The only SiC/SiC material being commercially introduced into aircraft engines is GE's HiPerComp™ manufactured via MI [13]. Research programs conducted at NASA Glenn Research Center showed

\* Corresponding author.

E-mail addresses: [yuanshi@outlook.de](mailto:yuanshi@outlook.de), [yuyuan.shi@dlr.de](mailto:yuyuan.shi@dlr.de), [yuan.shi@dlr.de](mailto:yuan.shi@dlr.de) (Y. Shi).

<sup>1</sup> These two authors contributed equally to this article.

that MI based SiC/SiC components have excellent strength at room temperature (RT) and high temperature (HT). They show good creep properties and long-term stability up to 1315 °C [2,9,14]. An alternative silicon free SiC/SiC composite described DiCarlo [2] manufactured via CVI or PIP processing or a combination of both [15].

The mechanical behavior of CVI SiC/SiC is well described in literature, while there is only little information found about the mechanical behavior at HT of SiC/SiC manufactured via PIP. Off-axis ( $\pm 45^\circ$ ) HT tensile tests of composites with third generation SiC fibres in SiCN matrix have not been found in literature. Kohyama et al. tested a PIP SiC/SiC material based on first generation SiC fibres (Tyranno LoxM) at temperatures up to 1400 °C in air, which showed a strength reduction of more than 30 % [16]. Davies et al. measured an even higher strength reduction for Tyranno LoxM based PIP material derived from polytitanocarbosilane precursor at 1380 °C in vacuum [17]. Nozawa et al. performed tensile tests at RT in on-axis (0/90 °) and off-axis ( $\pm 45^\circ$ ) orientation on PIP SiC/SiC samples based also on Tyranno LoxM fibres and the results showed that the tensile properties of the composites with the same axial fiber volume content were independent of the specimen size [18]. Rajan et al. performed tensile tests at RT for PIP material with Hi-Nicalon fibres and SiCN matrix showing a much lower tensile strength in  $\pm 45^\circ$  than in 0/90 ° orientation [19].

This work is focusing on the characterization of PIP derived SiC/SiCN material. The polysilazane based SiCN matrix was reinforced with high quality third generation Tyranno SA3 fibres (plain weave fabrics) and the SiCN matrix contains ~ 25 at% nitrogen and ~ 30 at% carbon. Compared to the use of polycarbosilanes which convert into SiC ceramics, it was found elsewhere that the use of polysilazanes has advantages in terms of lower raw material costs and shorter process times [11]. Previous material variants showed good mechanical properties at RT and in 0/90 ° orientation and sufficient damage tolerance without any additional fibre coating. However, the SiC/SiCN composites were only tested previously at RT and in 0/90 ° orientation. The manufacturing and characterization of microstructure and pore distribution of this material is described in detail elsewhere [11,20,21]. The effect of temperature and fibre orientation on the mechanical properties as well as residual thermal stresses are investigated in this work. Furthermore, temperature dependent thermal properties such as coefficient of thermal expansion and thermal conductivity are determined. In order to understand the role of matrix for the damage tolerance of the SiC/SiCN composite and for the behaviour under tensile load in 0/90 ° direction, additionally tensile tests were performed in  $\pm 45^\circ$  orientation, both at RT and HT. HT tensile tests were carried out at 1300 °C, which is the maximum manufacturing temperature. The tensile tests (RT and HT) were performed under quasi-static and loading-unloading modes which allows calculation of residual thermal stresses. The in-plane shear modulus of on-axis and off-axis orientations were determined through Iosipescu-method at RT. Obtaining comprehensive experimental data and an in-depth understanding of the material behavior are of great interest for the further material development and the material-appropriate design of components.

## 2. Material and methods

### 2.1. Material SiC/SiCN

A SiC/SiCN composite plate with the final dimensions of  $280 \times 190 \times 4 \text{ mm}^3$  was manufactured using the PIP method. First, 24 layers of Tyranno SA3 plain weave fabrics ( $300 \times 200 \text{ mm}^2$ , UBE Industries, LTD, Japan) were stacked and infiltrated via resin transfer molding (RTM). Polysilazane Durazane 1800 (Merck KGaA, Germany) was used as matrix precursor and no fibre coating was applied. As curing agent 1 wt. % of dicumyl peroxide (Alfa Aesar, Germany) was mixed with the resin before infiltrating the resin into the fibres at 80 °C. Curing was performed at 260 °C in nitrogen atmosphere with a pressure of 20 bar. During pyrolysis at 1300 °C in nitrogen atmosphere (1 bar) the polymer

matrix converts into a ceramic SiCN matrix. Due to the volume shrinkage of the matrix, porosity and matrix cracks are formed. In order to reduce the open porosity a total number of seven PIP cycles were performed. The manufacturing process is described in detail elsewhere [20,22]. After the final pyrolysis, the thickness of the plate was 4.4 mm. The surface was then grinded from both sides to a final thickness of 4 mm.

### 2.2. Material characterization

The fibre volume content of the manufactured SiC/SiCN plate was calculated by the initial weight of the SiC fibres and the total volume of the finished composite in as manufactured state. Density and porosity of the manufactured plate material were measured using Archimedes method according to standard DIN EN 1389. The coefficient of thermal expansion (CTE) was measured via high temperature dilatometry (Netzsch GmbH, Germany) in on-axis (0/90 °) and off-axis ( $\pm 45^\circ$ ) orientations according to DIN EN 1159-1:2003. For each orientation three samples with dimensions  $4 \times 5 \times 25 \text{ mm}^3$  were measured from 200 °C up to 1460 °C, and the mean value was calculated from three measurements. Taking into account the temperature dependent specific heat capacity ( $C_p$ ) of the material, laser flash analysis (LFA) was used to determine thermal conductivity ( $\lambda$ ) between 23 °C and 1000 °C (LFA 457, Netzsch GmbH, Germany). Sample dimensions were 12.6 mm in diameter with a thickness of 2.5 mm. A Pyroceram 9606 sample was used as reference material. Two samples were measured with three measurements per temperature step for each sample.

Polished samples of the material in as manufactured state and fracture surfaces of the tested tensile specimens were analyzed by scanning electron microscopy (SEM, Gemini Ultra Plus, Carl Zeiss NTS GmbH, Germany) and Energy-Dispersive X-ray spectroscopy (EDS, X-Max20, Oxford Instruments, United Kingdom).

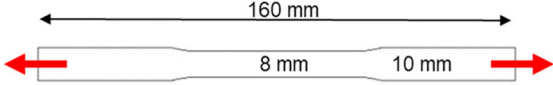
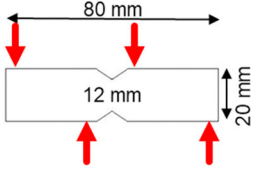
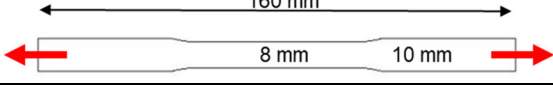
Table 1 gives an overview of the performed mechanical tests and the according standards, specimen size and the loading direction. The coupons for the tests were cut from a flat plate with thickness of 4 mm and in two directions for the mechanical tests with fibre orientation of 0/90 ° and  $\pm 45^\circ$ .

The mechanical properties at RT, including elastic and shear moduli ( $E$  and  $G$ ), Poisson's ratio ( $\nu$ ), strength ( $\sigma$ ) and failure strain ( $\epsilon$ ) were measured under uniaxial quasi-static tensile and Iosipescu-shear loading in fibre orientations 0/90 ° and  $\pm 45^\circ$ , respectively. The experiments were performed up to failure on a universal testing machine (Zwick 1494) at a controlled cross head speed of 1 mm/min. For the tensile tests, the longitudinal and transverse strains were measured with strain gauges. During Iosipescu-shear tests, strain was measured with strain gauges in  $+45^\circ$  and  $-45^\circ$  directions relative to the shear loading direction.

For HT tests dog-bone tensile specimens (see Table 1) were used at 1300 °C under nitrogen atmosphere. The HT tests were performed with a loading rate of 0.5 mm/min in a universal testing machine Zwick/Roell 1465 equipped with a vacuum chamber and an induction unit EMA HG1-DS (EMA Indutech GmbH, Germany). The longitudinal strain at HT was measured using a laser extensometer P-50 (Fiedler Optoelektronik, Germany). Furthermore, tensile specimens were used for cyclic loading-unloading tests (compliance tests) at RT and HT. For the tests at RT, first cycle was performed up to 30 MPa. After unloading with same crosshead speed close to zero, the load was increased in each following loading step by 30 MPa up to final rupture of specimen. Considering the results under quasi-static loading (details are provided in Section 3.2), the first loading-unloading cycle was performed up to 100 MPa with incremental loading steps of 50 MPa per cycle for 0/90 ° specimens at HT. For  $\pm 45^\circ$  specimens the first cycle was chosen up to 60 MPa with loading steps of 20 MPa per cycle. For statistical confirmation at least three samples per series were tested.

**Table 1**

Specimen geometry with dimensions (thickness of 4 mm), loading direction regarding to fibre orientation ( $0/90^\circ$  and  $\pm 45^\circ$ ) for different mechanical tests at RT and  $1300^\circ\text{C}$ , and the associated DIN EN standards.

Test	Standard	Specimen geometries, dimensions and loading direction
Tensile test at RT (Quasi static and cyclic loading-unloading)	DIN EN 658-1: 1999	
Iosipescu-shear test at RT	DIN EN 12289: 2005	
Tensile test at $1300^\circ\text{C}$ (Quasi static and cyclic loading-unloading)	DIN EN 1892:2005	

### 3. Results

#### 3.1. Material properties and microstructure

Fibre volume content, open porosity and density of the investigated SiC/SiCN material are 42.0 %, 5.9 % and  $2.5\text{ g/cm}^3$ , respectively. The temperature dependent CTE in on-axis ( $0/90^\circ$ ) and off-axis ( $\pm 45^\circ$ ) orientation is shown in Fig. 1. In  $0/90^\circ$  orientation the CTE increases almost linearly from  $2.9 \times 10^{-6}/\text{K}$  to  $5.2 \times 10^{-6}/\text{K}$  between  $200^\circ\text{C}$  and  $1400^\circ\text{C}$ . In comparison, the value in off-axis direction is slightly higher for  $4.3 \times 10^{-6}/\text{K}$  at  $200^\circ\text{C}$  and  $8.0 \times 10^{-6}/\text{K}$  at  $1400^\circ\text{C}$ . The difference of CTE in on-axis and off-axis directions probably relates to the interaction between the specific fibre orientation and the contribution of the matrix. Although the CTE and the elastic properties of the fibre in as-received condition are well known, it is still difficult to make a statement about the measured CTE values due to the lack of data concerning fibre and matrix properties within composite. Further investigation on SiCN-based composites is ongoing and the results will be published in the near future.

The thermal conductivity ( $\lambda$ ) perpendicular to the laminate plane and the specific heat capacity ( $c_p$ ) of investigated SiC/SiCN were measured in thru thickness direction and the results are shown in Fig. 2. The  $c_p$  was measured directly by means of differential scanning calorimetry (DSC) in the temperature range of  $50\text{--}550^\circ\text{C}$ . In the range of RT to  $1000^\circ\text{C}$   $c_p$  values were determined indirectly by LFA method by measuring the thermal diffusivity and comparing it with a Pyroceram 9606 reference material. Both methods result in similar  $c_p$  values, which are comparable to those of monolithic SiC [23]. This means that the performed LFA method for determining  $c_p$  and  $\lambda$  is reasonable and the

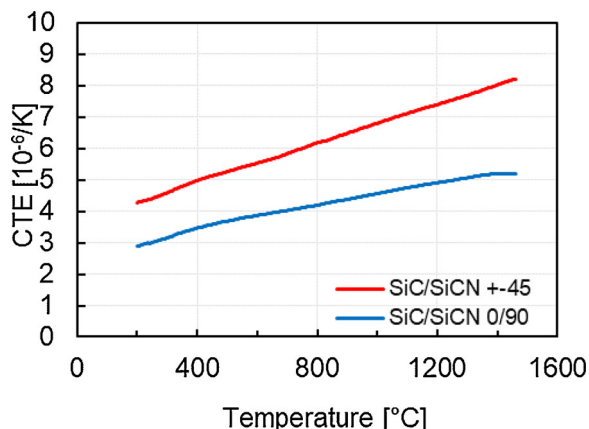


Fig. 1. Temperature dependent CTE in different fibre orientations of SiC/SiCN.

values can be trusted. The thermal conductivity increases slightly from  $2.8\text{ W/mK}$  at RT to  $3.3\text{ W/mK}$  at  $1000^\circ\text{C}$  which is a bit lower compared to 3D SiC textured PIP SiC/SiC material ( $3.7\text{ W/mK}$  at RT and  $4.9\text{ W/mK}$  at  $1100^\circ\text{C}$ ) from the work of Yamada et al. [24], due to its reinforcement of SiC fibre in thru thickness direction. Furthermore, the thermal conductivity of SiC/SiCN is considerably lower compared to melt infiltrated SiC/SiC material (e.g.  $24.7\text{ W/mK}$  at RT [7]), which is explained by the amorphous matrix and the high porosity in the PIP matrix [25–27].

The SEM pictures in Fig. 3 show the microstructure of SiC/SiCN. Areas with large pores, pore clusters and meso-cracks can be found in between the fibre bundles (Fig. 3a). Inside the fibre bundles, SiCN matrix segments can be observed (Fig. 3b and c). These segments result from the re-infiltration cycles during PIP. The EDS mapping reveals some oxygen impurity in the SiCN matrix which concentrates at the matrix interfaces between PIP cycles and also between matrix and fibres (Fig. 3d–g). Mainzer et al. explained this with the handling of the composites in air [11]. Furthermore, the previous analysis using X-ray diffraction method showed that the SiCN matrix is amorphous and remains stable up to  $1500^\circ\text{C}$  in nitrogen atmosphere. Crystallization of SiC and  $\text{Si}_3\text{N}_4$  only occurs at temperatures above  $1500^\circ\text{C}$  [11,20].

#### 3.2. Results of mechanical tests

Typical tensile stress-strain curves with quasi static loading and loading-unloading cycles of SiC/SiCN with fibre orientation of  $0/90^\circ$  and  $\pm 45^\circ$  are shown in Fig. 4 for RT and  $1300^\circ\text{C}$ . The indices T, R, “Comp” and “1300” denote the tensile test, room temperature, compliance test and  $1300^\circ\text{C}$ , respectively. The stress-strain response strongly depends on the loading direction. With  $0/90^\circ$  orientation, the composite shows only a slight non-linear behavior with high strength at RT (Fig. 4a), because the loading direction is aligned with fibre orientation. In contrast, the SiC/SiCN with orientation of  $\pm 45^\circ$  shows a clear non-linear behavior and low strength. Similarly, the ultimate stress of  $\pm 45^\circ$  at  $1300^\circ\text{C}$  is significantly lower than ultimate stress of  $0/90^\circ$ . For  $\pm 45^\circ$  orientation a strong nonlinear stress-strain curve is observed in Fig. 4b. At high temperature, a laser extensometer was used which allows strain measurement only in one direction. Thus, only the strain in longitudinal direction (loading direction) was measured at HT (Fig. 4b).

The loading and unloading cycles (compliance tests) at RT (Fig. 4a) show hysteresis loops, however, no permanent strain are determined for both fibre orientations. In contrast, at  $1300^\circ\text{C}$  the permanent strain increased with number of cycles especially in case of fibre orientation  $\pm 45^\circ$  (Fig. 4b). The stress-strain behavior under quasi-static and under compliance loading are comparable for both orientations at RT (Fig. 4a) or  $1300^\circ\text{C}$  (Fig. 4b) indicating that compliance tests do not change the stress-strain response compared to monotonic loading.

The mean value and standard deviation of tensile properties of SiC/

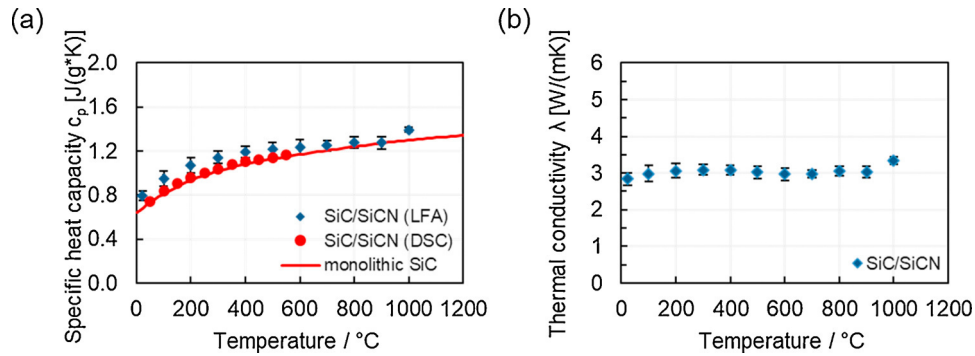


**Fig. 2.** Temperature dependent specific heat capacity (a) and thermal conductivity (b) of SiC/SiCN material measured by means of laser flash analysis (LFA). Specific heat capacity (a) is compared to measurements by means of differential scanning calorimetry (DSC) and literature values for monolithic SiC [23].

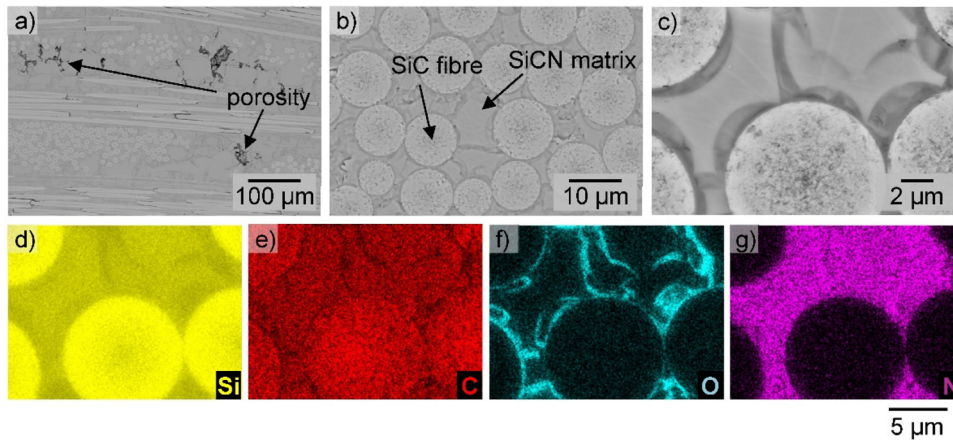


**Fig. 3.** Microstructure of SiC/SiCN, (a) to (c) SEM images and (d) to (g) element maps measured via EDS.

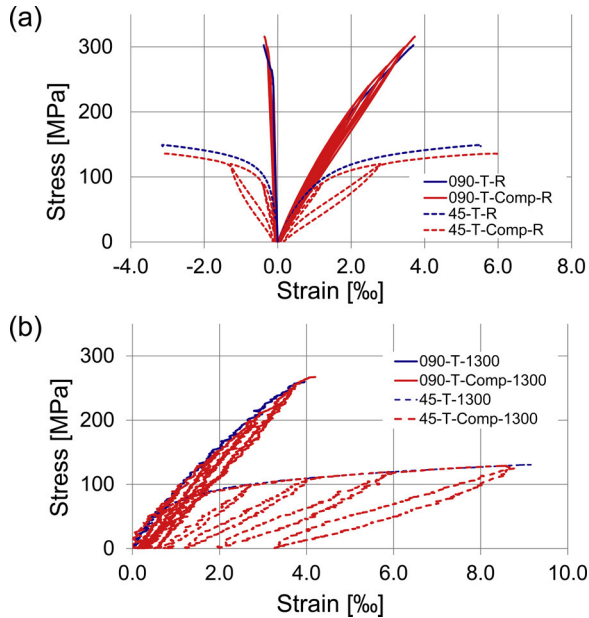


**Fig. 4.** Typical tensile stress-strain curves of SiC/SiCN with fibre orientation 0/90 ° and ±45 ° under quasi static loading and compliance loading a) at RT and b) at 1300 °C. The index T, R, “Comp” and “1300” denote the tensile test, room temperature, compliance test and 1300 °C, respectively.

**Table 2**

Summary of Young’s modulus, shear modulus, strength values and fracture strain obtained from tensile and Iosipescu-shear tests at RT and 1300 °C. The samples were prepared from a flat plate and tested with fibre orientation of 0/90 ° and ±45 °.

Tensile loading	Strength [MPa]	Young’s modulus [GPa]	Fracture strain [%]	Poisson’s ratio [-]
0/90 ° at RT	293.9 ± 16.6	140.0 ± 5.8	3.5 ± 0.3	0.11 ± 0.01
±45 ° at RT	141.8 ± 6.8	138.1 ± 31.2	5.2 ± 1.0	0.36 ± 0.16
0/90 ° at 1300 °C	262.9 ± 9.4	100.8 ± 4.7	3.9 ± 0.3	–
±45 ° at 1300 °C	128.7 ± 2.1	105.0 ± 9.2	8.4 ± 0.8	–
Iosipescu-shear loading	Strength [MPa]	Shear-modulus [GPa]	Fracture strain [%]	
0/90 ° at RT	103.3 ± 5.6	100.5 ± 6.1	7.8 ± 0.1	
±45 ° at RT	–	121.0 ± 29.4	–	

SiCN with fibre orientation 0/90 ° and ±45 ° at RT and 1300 °C are summarized in Table 2. The determination of the Young’s modulus was conducted using a linear fit of the initial linear region of the stress-strain curves under quasi-static loading, and using a linear fit of the linear region at first cycle of compliance test. The strength value was calculated from the maximum load according to the related standards and the fracture strain was defined as the strain value at strength. As the values of the quasi-static and the compliance tests at RT and 1300 °C are highly comparable, it is obvious that the compliance test does not influence the mechanical properties of SiC/SiCN. Similar results of C/C-SiC material have been reported previously in [28]. Hence, the mean values of the



tensile tests in Table 2 were calculated from both quasi-static and compliance results.

The in-plane shear properties measured with Iosipescu-test at RT for on-axis and off-axis orientation are also summarized in Table 2. It should be pointed out that, in case of 0/90° the fracture path is between the two notches. In contrast, the fracture of ±45° specimens generally starts at one notch and propagates along the fibre orientation (+45° or -45° to the loading direction), which indicate invalid failure according to DIN EN 12289: 2005. But as the necessary stress-strain curve for the determination of the shear modulus only relates to the initial linear region, the determined shear modulus of ±45° could surely be documented as characteristic value of the composite. The shear fracture strength and the ultimate strain are not discussed in this work.

## 4. Discussion

### 4.1. New approach for classification of WMC and WIC and assignment of the SiC/SiCN

Compared to high-performance monolithic ceramics, the most distinguishing characteristic of CMCs is their quasi-ductile deformation behavior, due to mechanisms such as fibre pull-out and multiple matrix cracking. This can be explained by a relatively weak bonding between fibre and matrix [29]. In general, there are two concepts that allow non brittle fracture behavior: either mechanically weak fibre coatings for Weak Interface Composites (WIC) or a weak matrix for Weak Matrix Composites (WMC). WIC typically have a dense matrix but a weak fibre-matrix interface in order to allow debonding between fibres and matrix, which increases the fracture toughness of the composites [30]. In contrast, WMC have a weak and compliant matrix, which enables crack propagation and deflection within the matrix [31]. Concerning crack propagation mechanisms, the brittle or non-brittle failure mode can be directly connected to the relative fracture energy of interface and fibre  $\Gamma_I/\Gamma_F$  and the relative stiffness of fibre and matrix  $(E_F - E_M)/(E_F + E_M)$  [32]. In the case of WIC, the Young's modulus of matrix and fibre are usually in the same range, therefore the fracture energy of the interface relative to the fibres must be rather low (e.g.,  $\Gamma_I/\Gamma_F < 0.25$ ) to prevent brittle failure. With WMC, stiffness of matrix is usually much lower than stiffness of fibre, thus the properties of the relative fracture energy of interface and fibre plays a minor role.

However, due to the lack of data concerning fibre and matrix properties within the composite material, the determination of fracture energies and of Young's modulus values is particularly difficult. After the complex manufacture processing of CMCs, the microstructure of the matrix, such as micro-crack density and specific matrix-porosity, are totally different from pure matrix properties and also depend on the fibre orientation. On the other hand, the material properties of fibres within the composite are unknown since they may differ from their original state as a result of the thermal load during fabrication of the composite. Furthermore, the original conditions of WMC and WIC concepts defined in [30,32] should be only considered as distinctive boundary cases, while most CMCs are normally located somewhere between them. As discussed above, in order to avoid brittle failure, at least one of the CMC components has to be weak enough to allow debonding and/or propagation of cracks, such as weak interface in WIC or weak matrix in WMC. Since the properties of each component not only depend on the choose of raw materials but also on e.g., manufacturing route, porosity, and others, the definition of WIC and WMC simply according to the stiffness ratio of 0/90° and ±45° orientation [32] may not be appropriate enough for some CMCs.

Countering the above discussed drawbacks, a new approach for classification of WMC and WIC is proposed in this work with consideration of the characteristic different properties between on-axis (orientation of fibre in loading direction) and off-axis loading. Instead of using individual properties of fibre, matrix and interface, the proposed idea uses the ratio of Young's modulus and strength from composite in 0/90°

and ±45° orientation, since the stiffness in 0/90° orientation is considered to be fibre dominated direction while in ±45° the matrix is dominant. The new approach can be considered as a supplement to the previous classification, where only the Young's modulus is considered [32]. Furthermore, as the fracture energy strongly depends on the load-bearing capacity of material, the strength values under on-axis and off-axis loading are considered to be in direct correlation to the fracture energy of both orientations.

According to this new approach, the CMCs with high strength ratio  $\sigma_{0/90^\circ}/\sigma_{\pm 45^\circ}$  and high stiffness ratio  $E_{0/90^\circ}/E_{\pm 45^\circ}$  should be classified to the WMCs, since the mechanical properties are significantly reduced under off-axis loading and the fibres cannot carry the load sufficiently. In other words, the mechanical performance of WMC is strongly influenced by the fibre properties and depends on the orientation and content of fibres. Thus, it can be assumed that strength and stiffness will significantly decrease if the loading direction differs from the fibre orientation. Furthermore, in case of CMCs with weak matrix, the strength ratio  $\sigma_{0/90^\circ}/\sigma_{\pm 45^\circ}$  will increase as the stiffness ratio grows. The infiltration or impregnation processes (e.g., polymer infiltration and slurry impregnation) to prepare the CMC-matrix could provide a high and fine porosity, which leads to low strength and low Young's modulus of matrix compared to that of the fibre. In this case, a non-brittle failure of the composite should be still achievable even if the fibre-matrix-interface is strong. But even if both ratios of WMCs are high, an excessively higher strength and Young's modulus of 0/90° orientation compared to the ±45° will not be observed, as in this case the matrix-related properties (e.g., interlaminar strength) are too weak. Therefore, it is reasonable to assume that a large difference between on-axis and off-axis loading is not to be expected.

CMCs with low strength ratio  $\sigma_{0/90^\circ}/\sigma_{\pm 45^\circ}$  and low stiffness ratio  $E_{0/90^\circ}/E_{\pm 45^\circ}$  can be defined as WIC in the proposed classification. Since the matrix of WIC is denser, stronger and stiffer, which leads to the similar properties of fibre and matrix, the mechanical performance (both Young's modulus and strength) of WIC is relatively insensitive to fibre orientation and loading type. The fibre coating is usually inevitable for the non-brittle failure of WIC and also responsible for the nonlinear stress-strain-curve resulting from fibre matrix debonding after matrix cracking. As in general a completely dense matrix cannot be achieved, the mechanical properties of matrix within composite usually will not be higher than the values of fibre. Therefore, equal Young's modulus and strength in on-axis and off-axis directions can be defined as threshold value, both ratios should not be lower than 1. Though the definition of a dividing-line between WIC and WMC is practically difficult, it is assumed that the WIC are gathered within a relatively small area.

In order to verify the proposed approach, the ratio of strength  $\sigma_{0/90^\circ}/\sigma_{\pm 45^\circ}$  and stiffness  $E_{0/90^\circ}/E_{\pm 45^\circ}$  in on-axis and off-axis orientations of the investigated SiC/SiCN material, and several other CMCs from various sources were calculated. Their values are ranked as a measure of classification to WIC and WMC and summarized in Fig. 5 and the relevant properties which were available from literature are listed in Table 3.

Firstly, the CMCs with considerably high porosity, e.g., C/C with 10–12 % [32] as well as several oxide CMCs with more than 20 % [33–35], show relatively high strength ratio  $\sigma_{0/90^\circ}/\sigma_{\pm 45^\circ}$  and stiffness ratio  $E_{0/90^\circ}/E_{\pm 45^\circ}$  (blue symbols in Fig. 5). Such materials can be defined as WMC. WMC can be found in a relatively big area (blue shaded). This tendency is visualised in Fig. 5 indicating that the strength ratio increases with increasing stiffness ratio. This confirms the above-mentioned approach with the highest values of strength and Young's modulus ratios from material C/C SIGRABOND [32] are approx. 6 and 4, respectively.

CMCs with denser matrix and with weak interface are grouped together as WIC shown in Fig. 5 as red symbols. Their  $\sigma_{0/90^\circ}/\sigma_{\pm 45^\circ}$  and  $E_{0/90^\circ}/E_{\pm 45^\circ}$  ratios are clearly lower, e.g., Nicalon SiC/SiC composites [36] show values close to 1, due to similar mechanical properties of fibre and matrix. In this case, a non-brittle failure of composite is achieved

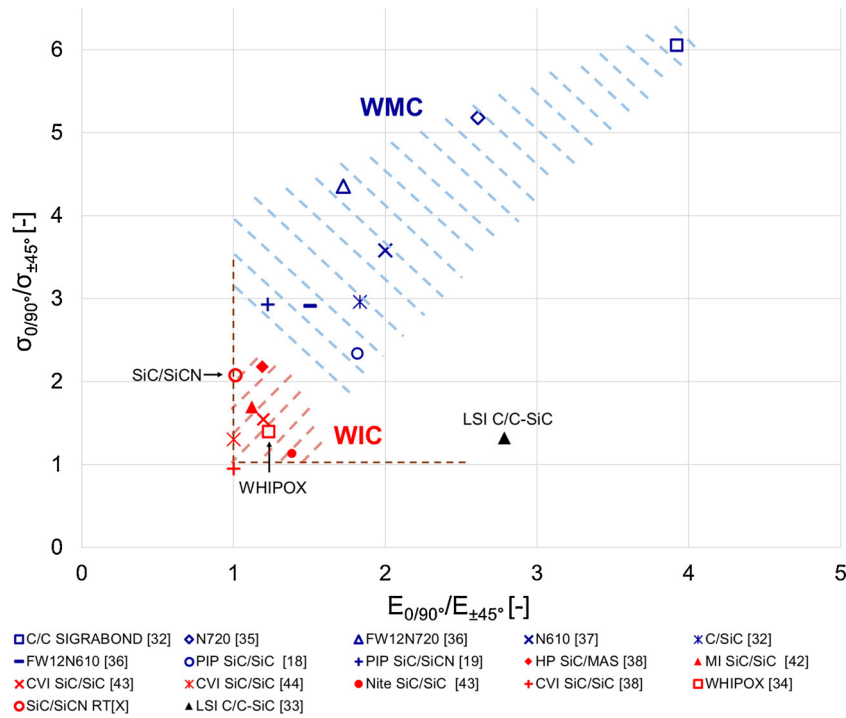


Fig. 5. Classification of different CMCs to WMC or WIC concept according to the ratio of Young's modulus  $E_{0/90^\circ}/E_{\pm 45^\circ}$  and strength  $\sigma_{0/90^\circ}/\sigma_{\pm 45^\circ}$ . Results from literature and own measurements of SiC/SiCN at RT (marked with [X]).

Table 3

Relevant properties and manufacturing methods of various CMCs classified as WMC (blue), WIC (red) and one exception LSI C/C-SiC (black) in Fig. 5 (as far as available from literature) [32,33,34,35,32,34,18,19,36,42–44,43,36–38].

	Material	Manufacturing method
C/C SIGRABOND [32]	C/C SIGRABOND 1501 G, 24 layers, open porosity 10–12 %	Liquid polymer infiltration
N720 [33]	Nextel 720/mullite and alumina, 12 layers, fibre content 39 % and matrix porosity 38 %	Ceramic slurry impregnation (1200°C)
FW12N720 [34]	Nextel 720/Al <sub>2</sub> O <sub>3</sub> -SiO <sub>2</sub> -ZrO <sub>2</sub> , 12 layers, fibre content ca. 40 % and open porosity of the composite 34 %	Slurry infiltration and sintering (1000°C-1300°C)
N610 [35]	Nextel 610/80% mullite and 20% alumina, composite porosity 22–25% and matrix porosity 38–42%	Ceramic slurry impregnation (1200°C)
C/SiC [32]	T800 C/SiC, 4 UD layers	Liquid polymer infiltration
FW12N610 [34]	Nextel 610/Al <sub>2</sub> O <sub>3</sub> -SiO <sub>2</sub> -ZrO <sub>2</sub> , 12 layers, fibre content ca. 40 % and open porosity of the composite 28 %	Slurry infiltration and sintering (1000°C-1300°C)
PIP SiC/SiC [18]	Tyranno-Loxm fibre, Plane-weave, porosity above 20 %	Polymer impregnation and pyrolysis
PIP SiC/SiCN [19]	Hi-Nicalon SiC/SiCN, 8-harness satin weave with BN/Si <sub>3</sub> N <sub>4</sub> coating	Precursor impregnation pyrolysis
HP SiC/MAS [36]	Nicalon SiC/MAS 12 layers, fibre content 40 %, fully dense MAS matrix	Hot pressing
MI SiC/SiC [42]	Sylramic-iBN SiC/SiC, fibre content 36-39 %, closed porosity 5 %, multilayered interface coating,	Melt infiltration
CVI SiC/SiC [43]	Tyranno SA3 SiC/SiC, plain weave, fibre content 30 %, porosity 10-20%, PyC interface coating	Chemical vapor infiltration
CVI SiC/SiC [44]	Nicalon SiC/SiC, plain weave, fibre content 35 %, porosity 10–15 %, PyC interface coating	Chemical vapor infiltration
Nite SiC/SiC [43]	Tyranno SA3 SiC/SiC, plain weave, fibre content 30 %, dense matrix, PyC interface coating	NITE
CVI SiC/SiC [36]	Nicalon SiC/SiC, fibre content 32 %, matrix porosity 8.6 %	Chemical vapor infiltration
LSI C/C-SiC [37]	T800 C/C-SiC, fibre content 60 %, open porosity 1.2 %	Liquid silicon infiltration
WHIPOX [38]	Nextel 610/Al <sub>2</sub> O <sub>3</sub> , fibre content 40.5 %, open porosity 29.1 %	Winding and sintering 1300°C
PIP SiC/SiCN RT[X]	Tyranno SA3 SiC/SiCN, plain weave, fibre content 42 %, open porosity 5.9 %, no interface coating	Polymer Infiltration and pyrolysis

through fibre coating (e.g., BN, PyC or combination of several interfaces, etc. in Table 3). As discussed above, due to the fact that the strength and stiffness of matrix would not be greater than that of the fibres, two borderlines with a value of 1 for both axes are adjusted in Fig. 5. The WIC are found in the red shaded area with a stiffness ratio between 1 to approx. 1.5 and strength ratio 1 to approx. 2, which agrees well with the above proposed approach.

Compared to the original conditions of WMC and WIC concepts, the new classification can be realized by ratios of Young's modulus and strength from composites loaded in 0/90 ° and ±45 ° orientation, respectively. It seems to be reasonable for most CMCs except LSI C/C-SiC [37] (black symbols in Fig. 5). This composite shows features from both, WMC and WIC. Additionally, WHIPOX [38] and SiC/SiCN [X] (own measurements) show lower values, although no fibre coating was

applied. The special features of these three materials are closely related to their individual microstructure:

- The microstructure of LSI based C/C-SiC [37] is characterized by block-wise segmentations (so called “block structure”): within the quasi-rectangular C/C block, the carbon fibre bundles are embedded in the residual pyrolytic C-matrix; the C/C structures are surrounded by SiC-matrix; a defined interface (e.g. fibre coating) between fibre and matrix does not exist for C/C-SiC. The porous pyrolytic C-matrix could be the key reason for the lower Young’s modulus in  $\pm 45^\circ$  direction ( $E_{0/90^\circ}/E_{\pm 45^\circ}$  is approx. 2.8). The similar strength in on-axis and off-axis orientation ( $\sigma_{0/90^\circ}/\sigma_{\pm 45^\circ}$  is approx. 1.3) may be explained by the fibre bundle pull-out instead of single filament pull-out (fracture surfaces of  $0/90^\circ$  were reported in [28,39]), which could lead to a low utilization of fibre strength in  $0/90^\circ$  direction.
- WHIPOX (wound highly porous oxide matrix) reported in [38] consists of Nextel 610 fibre and  $Al_2O_3$  matrix and is produced by winding technique and sintering at  $1300^\circ C$ . Though the matrix porosity is rather high (approx. 30%), its distribution is not homogeneous: considerable agglomerations of matrix can be observed in [40]; repeated shrinkage cracks (approx. 8.7 per  $mm^2$ ) in meso-level are clearly visible for the orientation  $0/90^\circ$  ( $\pm 45^\circ$ ) [41]. Combined with these two factors, the local  $Al_2O_3$  matrix is dense and its mechanical properties could be comparable with those of the fibres. Furthermore, the connection between matrix and fibre maybe relative weak due to the shrinkage of matrix, which leads to a similar ratio of  $\sigma_{0/90^\circ}/\sigma_{\pm 45^\circ}$  and  $E_{0/90^\circ}/E_{\pm 45^\circ}$ . Further research is ongoing and will be published in the future.
- In case of SiC/SiCN (own measurements), no fibre coating is applied and the non-crystalline SiCN-matrix shows a relatively low porosity (approx. 5.9%). Furthermore, similar mechanical properties at RT in on-axis and off-axis orientation have been achieved as for other WIC. For explanation a new microstructure model is developed (see Section 4.2).

#### 4.2. Microstructure model of SiC/SiCN

The investigated SiC/SiCN material is produced with seven cycles of polymer infiltration and pyrolysis. During each pyrolysis step the polymer precursor decomposes and converts into SiCN matrix (Section

2.1). Because of the unhindered shrinkage and densification, the matrix is divided into many micro segments and each segment is then surrounded with the subsequent segments (Fig. 3c). Fig. 6a and b show detailed SEM images of the interface between SiC-fibre and SiCN-matrix and several initial cracks (red arrows) can be clearly observed. This indicates that the bonding between fibre and matrix is discontinuous. According to these distinguishing features of PIP manufacturing process, a microstructure model of SiC/SiCN is developed in Fig. 6c: the precursor of each process cycle shrank inwards from all directions (yellow arrows in Fig. 6c); the SiCN-matrix segmentations are shown with various colors; dark brown lines mark the initial cracks between fibre and matrix segments, and between two matrix segments of the last PIP cycle, which confirm with the SEM images in Fig. 6a and b.

In order to explain the material behavior of SiC/SiCN at RT with  $0/90^\circ$  and  $\pm 45^\circ$  orientation, a representative area of the microstructure model from Fig. 6c is used to explain crack development and crack distribution under different tensile loading states. The schematic representation is shown in Fig. 7.

Firstly, SiC/SiCN with fibre orientation of  $0/90^\circ$  is observed under tensile loading (Fig. 7, left). Due to the relatively small tensile force ( $F_1$ ), existing cracks do not grow significantly and no additional matrix cracks develop. Thus, the Young’s modulus can be evaluated in this initial linear region (elastic limit). Because of the discontinuous connection (Fig. 6) of fibre and matrix the bonding is extremely weak and the influence of different orientations  $0/90^\circ$  (Fig. 7, left) and  $\pm 45^\circ$  (Fig. 7, right) are considered to be insignificant in this initial region. Therefore, comparable Young’s modulus of both test directions at RT ( $E_{0/90^\circ}/E_{\pm 45^\circ}$  near to 1 in Fig. 5) are evaluated up to elastic limit without development of matrix cracks.

Then, as the force increases above a given applied stress ( $F_2$ ), the initial cracks will open and develop in both orientations. Because of the several densification cycles during the PIP manufacturing, it is reasonable to assume that the microstructure of SiCN matrix is inhomogeneous (Figs. 3c and 6 c). The interfaces between the segments resulting from different PIP cycles are potential debonding planes. Thus, in case of off-axis ( $\pm 45^\circ$  Fig. 7, right), more cracks between matrix segments will occur as the loading increases ( $F_i$ ). In contrast, since the loading direction is aligned with fibre orientation, the number of cracks in  $0/90^\circ$  orientation (Fig. 7, left) should be clearly smaller at same loading level.

Finally, matrix cracks develop as the load increases further. In  $0/90^\circ$

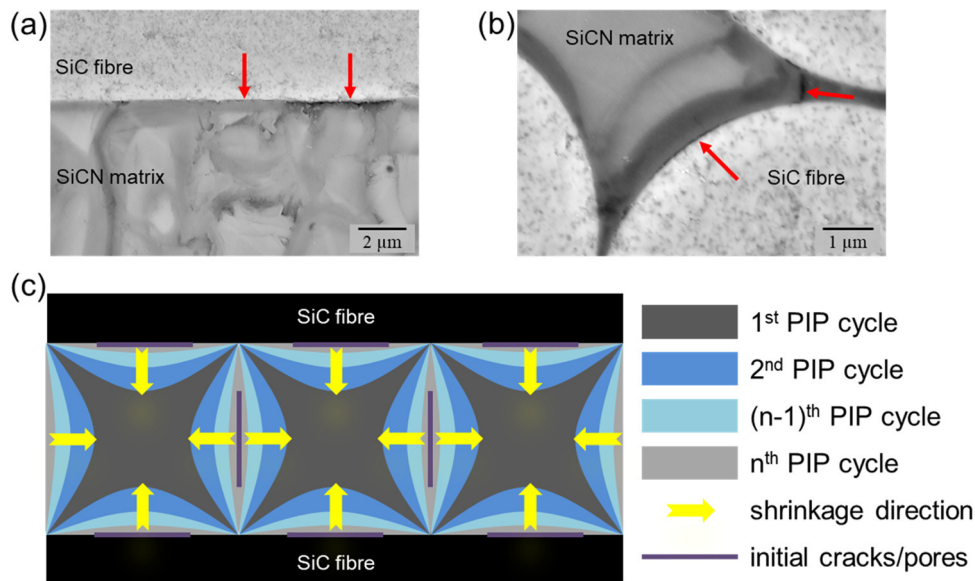


Fig. 6. (a) and (b) detailed SEM analysis of SiCN-matrix and interface between SiC-fibre and SiCN-matrix, several initial cracks are indicated with red arrows; (c) microstructure model of SiC/SiCN with consideration of shrinkage of each process cycle, formation of discontinuous SiCN-matrix segmentations and initial cracks/pores.



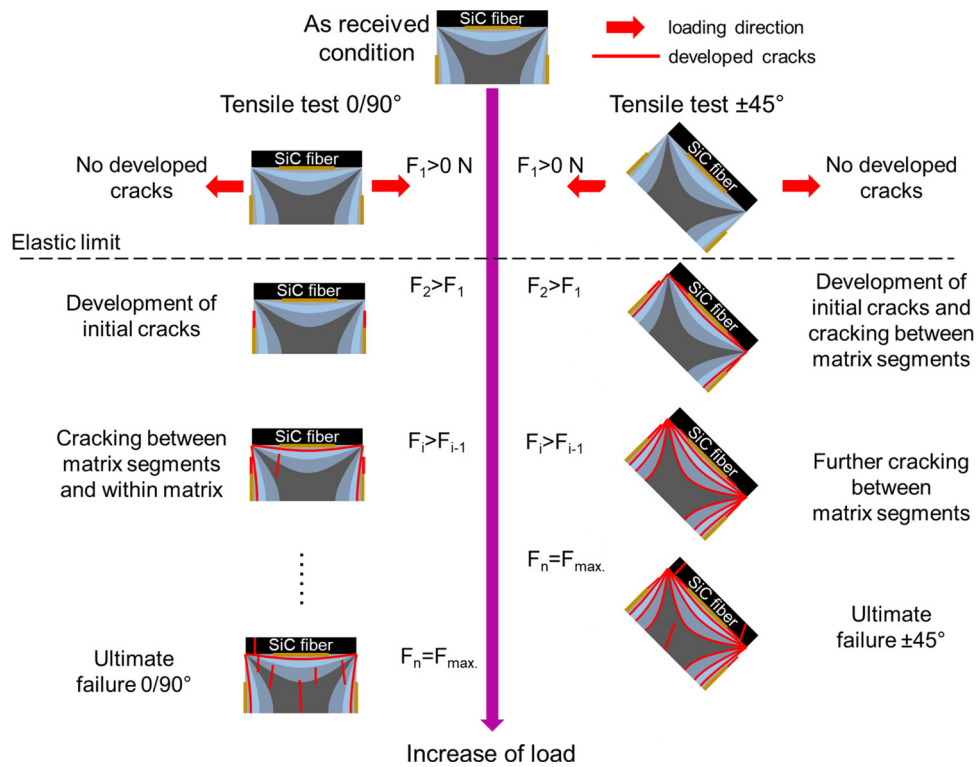


Fig. 7. Schematic representation of the crack development and distribution of SiC/SiCN with fibre orientation  $0/90^\circ$  and  $\pm 45^\circ$  under tensile loading at RT.

orientation the composite finally fails when loading exceeds the failure strain of fibre ( $F_n$ ). As the load-bearing capacity of SiC fibre is considerably stronger than the porous SiCN matrix, the strength of composite with orientation of  $0/90^\circ$  (fibre dominant) is higher than in  $\pm 45^\circ$  orientation (the ratio of  $\sigma_{0/90^\circ}/\sigma_{\pm 45^\circ}$  is approx. 2 in Fig. 5). In comparison, as matrix dominates the damage mechanism of  $\pm 45^\circ$  orientation, at failure ( $F_n$ ) the amount of developed cracks should be significantly higher than in  $0/90^\circ$  orientation, which leads to the clearly higher failure strains at  $\pm 45^\circ$  orientation (Table 2).

The fracture surfaces of the failed samples after tensile test were analyzed by SEM. A considerable difference can be observed between  $0/90^\circ$  (Fig. 8a and c) and  $\pm 45^\circ$  orientation (Fig. 8b and d). The fracture surfaces in matrix rich areas are rather smooth (Fig. 8a). This is also observed locally between fibres (Fig. 8c) at  $0/90^\circ$  tensile samples, which indicates that the cracks through segments are the dominant failure mechanism of SiCN matrix in this loading direction. This correlates well with the final crack distribution shown in the microstructure model of  $0/90^\circ$  (Fig. 7 left,  $F_n = F_{max}$ ). Compared to  $0/90^\circ$  orientation,

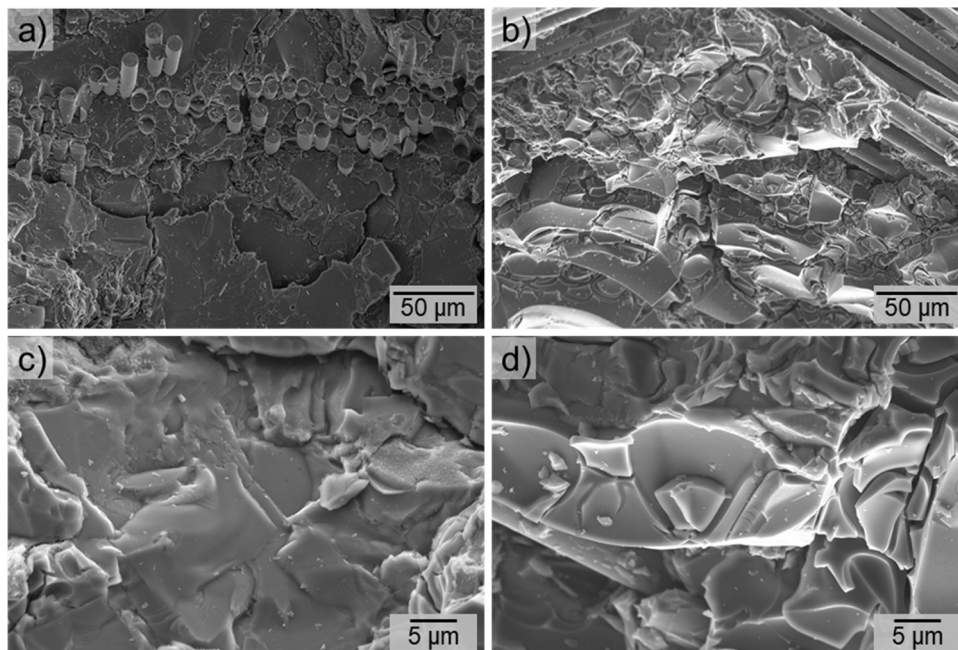


Fig. 8. SEM images for the fracture surface after tensile test at RT, (a) and (c) fibre orientation of  $0/90^\circ$ ; (b) and (d) fibre orientation of  $\pm 45^\circ$ .

the fracture surface of  $\pm 45^\circ$  is clearly wavy and the total number of matrix cracks is significantly higher than in case of  $0/90^\circ$  orientation. This explains the significantly higher failure strain of off-axis tensile loadings. Furthermore, enlargement of SEM in Fig. 8d shows distinctly shell-shaped cracks. This indicates that most cracks of  $\pm 45^\circ$  orientation appear and develop between matrix segments, which agrees strongly to the matrix failure mechanism of  $\pm 45^\circ$  orientation in the microstructure model (Fig. 7 right,  $F_n = F_{max}$ ).

#### 4.3. Effect of temperature on mechanical properties

The mechanical behavior of SiC/SiCN was investigated under tensile loading at  $1300^\circ\text{C}$ , which is the max. manufacturing temperature of the PIP process, and the characteristic values are summarized in Table 2.

As described in Section 3.2, almost no permanent strains under compliance test could be determined for both fibre orientations at RT. In contrast, at  $1300^\circ\text{C}$  the permanent strain increased with loading stress (Fig. 4). Through the extrapolation of the loading-unloading slopes (Fig. 4) of the top linear portion of each hysteresis loop, common intersection points can be found. The Y-axis values (stress) of intersection point in the stress-strain diagram are directly related to the residual thermal stresses (RTS) of composites [28,45,46]. This is shown in Fig. 9 for orientation of  $0/90^\circ$  at RT (Fig. 9a) and  $1300^\circ\text{C}$  (Fig. 9c),  $\pm 45^\circ$  at RT (Fig. 9b) and  $1300^\circ\text{C}$  (Fig. 9d). The detailed calculation procedure is introduced in previous publication [28]. At RT almost no RTS of SiC/SiCN can be calculated with  $0/90^\circ$  orientation (Fig. 9a) and  $\pm 45^\circ$  orientation (Fig. 9b). This can be explained by a release of thermal stress during several pyrolysis cycles, which led to micro cracks/pores within SiCN matrix. In contrast, for both loading orientations intersection points at  $1300^\circ\text{C}$  (Fig. 9c and d) indicate RTS, which could be induced by the mismatch of the coefficient of thermal expansion (CTE) of fibres and matrix at HT. According to the manufacture datasheet the CTE value of Tyranno SA3 fibre is  $4.5 \times 10^{-6} / \text{K}$  from RT to  $1000^\circ\text{C}$  [47]. A very comparable SiCN matrix material was investigated in [48] and its CTE is approx.  $3.5 \times 10^{-6} / \text{K}$ . Therefore, at high temperature this CTE mismatch between fibre and matrix leads to the development of RTS when heating up the SiC/SiCN. As a result, SiC fibre is under compressive stress and tensile stress exists in the SiCN matrix at  $1300^\circ\text{C}$ .

Since the amorphous state of SiCN matrix would not change up to  $1500^\circ\text{C}$  [11,20] and the properties of SiC fibre are stable at  $1300^\circ\text{C}$  in nitrogen atmosphere [49], the Young's modulus of SiC/SiCN composite should remain constant in the whole range from RT to  $1300^\circ\text{C}$ . However, clearly lower values of Young's modulus of same orientation at  $1300^\circ\text{C}$  are summarized in Table 2. As the SiCN matrix is under tensile

RTS at  $1300^\circ\text{C}$ , the elastic limit at HT, which is related to the onset of cracking of the matrix, should be much smaller compared to the elastic limit at RT. This leads to the results that the elastic properties at  $1300^\circ\text{C}$  cannot be evaluated from the region without development of matrix cracks.

Despite the difficulties of Young's modulus measurement at HT, the determined tensile strength and fracture strain at  $1300^\circ\text{C}$  are meaningful promising properties of SiC/SiCN (Fig. 10). Considering the standard deviation, the effect of temperature on tensile strength in both orientations is rather insignificant. The slightly lower strength values at HT could be explained by the RTS which causes matrix damage at  $1300^\circ\text{C}$ . The considerable increase of fracture strain at HT compared to RT can be observed in Fig. 10, especially for the orientation of  $\pm 45^\circ$ . According to the developed microstructure model in Figs. 6c and 7, the fibre-matrix-bonding is weak and the matrix consists of discontinuous micro SiCN segments. In this case, the present tensile RTS within matrix is smoothly released during mechanical testing at  $1300^\circ\text{C}$  and leads to an incomplete crack closure even after unloading, which can be confirmed through the clear permanent strain under compliance loading in both orientations (Fig. 9c and d). Moreover, the off-axis properties are dominated by matrix and compared to the  $0/90^\circ$  orientation, the total number of matrix cracks in  $\pm 45^\circ$  at  $1300^\circ\text{C}$  should be higher. Therefore, the fracture strain is higher (Fig. 10). In conclusion, since the strength ratio  $\sigma_{0/90^\circ} / \sigma_{\pm 45^\circ}$  is approx. 2 and Young's modulus ratio is approx. 1 (Table 2), the investigated SiC/SiCN at  $1300^\circ\text{C}$  still belongs to the WIC group.

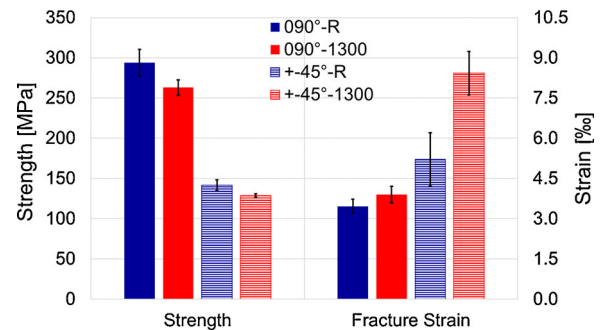


Fig. 10. Strength and fracture strain of SiC/SiCN material with fibre orientation of  $0/90^\circ$  and  $\pm 45^\circ$  under tensile loading at RT and  $1300^\circ\text{C}$ .

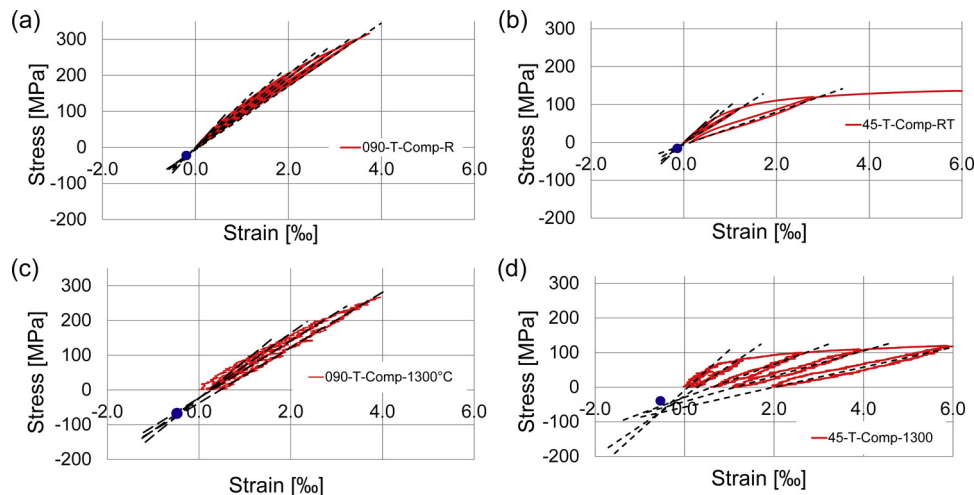


Fig. 9. Common intersection point (blue point) of SiC/SiCN compliance slopes by (a) orientation of  $0/90^\circ$  at RT; (b) orientation of  $\pm 45^\circ$  at RT; (c) orientation of  $0/90^\circ$  at  $1300^\circ\text{C}$  and (d) orientation of  $\pm 45^\circ$  at  $1300^\circ\text{C}$ .

## 5. Conclusions

In this work, the material properties of PIP based SiC/SiCN are investigated at RT and 1300 °C and a microstructure model is developed for the explanation of different mechanical behavior in on-axis and off-axis direction. Furthermore, a new approach for the classification of WIC- and WMC-concept is proposed according to the on-axis and off-axis properties of composite. The main conclusions are summarized:

- SiC/SiCN without fibre coating was manufactured using polymer infiltration and pyrolysis. A porosity lower than 6 % was achieved through 7 PIP cycles. The temperature dependent thermal conductivity and coefficient of thermal expansion was determined using laser flash analysis method and high temperature dilatometry.
- The relevant elastic constants, strength and fracture strain of SiC/SiCN are investigated in on-axis and off-axis directions under tensile and Iosipescu-shear loadings at RT. Through quasi-static and loading-unloading (compliance) tests, the tensile properties are then determined at 1300 °C, which corresponds to the manufacturing temperature of PIP process. Combined with the evaluated thermal properties, a material database of SiC/SiCN is established and can be employed as input for design of SiC/SiCN components.
- A new approach for the classification of WMC- and WIC-concept is proposed through the ratio of composite's properties between on-axis (0/90 °) and off-axis (±45 °) loading, instead of using the properties of fibre, matrix, and interface, which are not well measurable in practice. According to this new approach, the CMCs with high strength ratio  $\sigma_{0/90^\circ}/\sigma_{\pm 45^\circ}$  and stiffness ratio  $E_{0/90^\circ}/E_{\pm 45^\circ}$  are classified as WMCs. In case of CMCs with weaker matrix, the strength ratio  $\sigma_{0/90^\circ}/\sigma_{\pm 45^\circ}$  increases with increasing stiffness ratio. In contrast, WIC shows significantly lower ratios and they show values of stiffness ratio between 1 to approx. 1.5 and strength ratio 1 to approx. 2. This new classification of WMC and WIC is verified by the investigated SiC/SiCN and several other CMCs from other publications. It seems to be a reasonable approach for various CMCs and explains that CMCs with high porosity should not be intuitively defined as WMC. The distribution of pores and the inhomogeneity of matrix play an important role (e.g., WHIPOX). On the other hand, fibre coating is not the prerequisite of WIC: although no fibre coating is applied, similar mechanical properties of the investigated SiC/SiCN in on-axis and off-axis orientation can be achieved as for other WIC, which can be explained through the developed microstructure model. Because of its lower Young's modulus in ±45 ° direction and the dominating fibres in 0/90 ° direction, LSI C/C-SiC shows features of both WMC and WIC. The proposed approach is very helpful for the further development of CMCs to achieve a non-brittle fracture behavior through different strategies, as well as to optimize the manufacturing processing and material microstructure.
- Based on the analysis of the PIP induced SiCN matrix segments and the weak fibre-matrix-bonding, a microstructure model focusing on the crack propagation of SiC/SiCN under tensile loading is developed, which explains the material behavior and fracture mechanism of SiC/SiCN with different fibre orientations: comparable elastic properties but different strength and strain of both orientations at RT; smooth crack surface at 0/90 ° orientation and shell-shaped cracks between matrix segments at ±45 ° orientation. This model has been confirmed through the loading direction dependent test results and the analysis of fracture surface by SEM.
- The influence of temperature on the mechanical behavior of SiC/SiCN is determined by tensile tests conducted at RT and 1300 °C. Though the evaluation of Young's modulus at HT is unfeasible, the determined strength and fracture strain at 1300 °C are meaningful mechanical properties. Based on the analysis of tensile hysteresis measurements, the mismatch of CTE of fibre and matrix is considered as the key factor for different mechanical behaviors at RT and 1300

°C. Despite the slightly decreased strength value, the fracture strain of orientation 0/90 ° and ±45 ° increased significantly from RT to 1300 °C.

## Declaration of Competing Interest

The authors declare that they have no known competing financial interests or personal relationships that could have appeared to influence the work reported in this paper.

## Acknowledgments

This research is funded by German Aerospace Center (DLR). The authors like to thank Daniel Cepli and Dr. Martin Frieß at the DLR-Institute of Structures and Design for the collaboration and support for this work. We also thank Andrea Hanke from the DLR-Institute of Engineering Thermodynamics for the DSC measurement.

## References

- [1] N.P. Padture, *Advanced structural ceramics in aerospace propulsion*, *Nat. Mater.* 15 (8) (2016) 804–809.
- [2] J.A. DiCarlo, *Advances in SiC/SiC Composites for Aero-Propulsion*, National Aeronautics and Space Administration, Glenn Research Center, 2013.
- [3] D. Kopoliovich, *Advances in the manufacture of ceramic matrix composites using infiltration techniques*, in: I. Low (Ed.), *Advances in Ceramic Matrix Composites*, Elsevier, 2014, pp. 79–108.
- [4] A. Kohyama, *CMC for Nuclear Applications*, Ceramic Matrix Composites, Wiley-VCH Verlag GmbH & Co. KGaA, 2008, pp. 353–384.
- [5] Y. Katoh, L.L. Snead, C.H. Henager, A. Hasegawa, A. Kohyama, B. Riccardi, H. Hegeman, *Current status and critical issues for development of SiC composites for fusion applications*, *J. Nucl. Mater.* 367–370 (2007) 659–671.
- [6] B. Mainzer, K. Kelm, P. Watermeyer, M. Frieß, D. Koch, *How to Tame the Aggressiveness of Liquid Silicon in the LSI Process*, *Key Engineering Materials*, Trans Tech Publ, 2017, pp. 238–245.
- [7] G.S. Corman, K.L. Luthra, *Silicon melt infiltrated ceramic composites (HiPerComp™)*, in: N.P. Bansal (Ed.), *Handbook of Ceramic Composites*, Springer, Boston, MA, 2005, pp. 99–115.
- [8] B. Mainzer, R. Jemmali, P. Watermeyer, K. Kelm, M. Frieß, D. Koch, *Development of damage-tolerant ceramic matrix composites (SiC/SiC) using Si-BN/SiC/pyC fiber coatings and LSI processing*, *J. Ceram. Sci. Technol.* 08 (1) (2017) 113–120.
- [9] J. DiCarlo, H.-M. Yun, G. Morscher, R. Bhatt, *SiC/SiC composites for 1200°C and above*, in: N. Bansal (Ed.), *Handbook of Ceramic Composites*, Springer, 2005, pp. 77–98.
- [10] P. Colombo, G. Mera, R. Riedel, G.D. Soraru, *Polymer-derived ceramics: 40 years of research and innovation in advanced ceramics*, *J. Am. Ceram. Soc.* 93 (7) (2010) 1805–1837.
- [11] B. Mainzer, C. Lin, R. Jemmali, M. Frieß, R. Riedel, D. Koch, *Characterization and application of a novel low viscosity polysilazane for the manufacture of C- and SiC-fiber reinforced SiCN ceramic matrix composites by PIP process*, *J. Eur. Ceram. Soc.* 39 (2–3) (2019) 212–221.
- [12] F. Süß, T. Schneider, M. Frieß, R. Jemmali, F. Vogel, L. Klopsch, D. Koch, *Combination of PIP and LSI processes for SiC/SiC ceramic matrix composites*, *Open Ceram.* 5 (2021), 100056.
- [13] J. Steibel, *Ceramic matrix composites taking flight at GE Aviation*, *Am. Ceram. Soc. Bull.* 98 (3) (2019) 30–33.
- [14] M. Halbig, M. Jaskowiak, J. Kiser, D. Zhu, *Evaluation of ceramic matrix composite technology for aircraft turbine engine applications*, 51st AIAA Aerospace Sciences Meeting Including the New Horizons Forum and Aerospace Exposition (2013) 539.
- [15] J.A. Dever, M.V. Nathal, J.A. DiCarlo, *Research on high-temperature aerospace materials at NASA glenn research center*, *J. Aerosp. Eng.* 26 (2) (2013) 500–514.
- [16] A. Kohyama, M. Kotani, Y. Katoh, T. Nakayasu, M. Sato, T. Yamamura, K. Okamura, *High-performance SiC/SiC composites by improved PIP processing with new precursor polymers*, *J. Nucl. Mater.* 283 (2000) 565–569.
- [17] I.J. Davies, T. Ishikawa, M. Shibuya, T. Hirokawa, *Fibre strength parameters measured in situ for ceramic-matrix composites tested at elevated temperature in vacuum and in air*, *Compos. Sci. Technol.* 59 (6) (1999) 801–811.
- [18] T. Nozawa, Y. Katoh, A. Kohyama, *Evaluation of tensile properties of SiC/SiC composites with miniaturized specimens*, *Mater. Trans.* 46 (3) (2005) 543–551.
- [19] V.P. Rajan, J.H. Shaw, M.N. Rossol, F.W. Zok, *An elastic-plastic constitutive model for ceramic composite laminates*, *Compos. Part A Appl. Sci. Manuf.* 66 (2014) 44–57.
- [20] B. Mainzer, M. Friess, R. Jemmali, D. Koch, *Development of polyvinylsilazane-derived ceramic matrix composites based on Tyranno SA3 fibers*, *J. Ceram. Soc. Jpn.* 124 (10) (2016) 1035–1041.
- [21] B. Mainzer, *Entwicklung von keramischen SiC/SiC-Verbundwerkstoffen mit Tyranno SA3 Fasern auf Basis des PIP- und LSI-Verfahrens*, Karlsruhe Institut für Technologie, 2019.

- [22] S. Hönig, F. Süß, N. Jain, R. Jemmali, T. Behrendt, B. Mainzer, D. Koch, Evaluation of preparation and combustion rig tests of an effusive cooled SiC/SiCN panel, *Int. J. Appl. Ceram. Technol.* 17 (4) (2020) 1562–1573.
- [23] R. Brandt, M. Friess, G. Neuer, Thermal conductivity, specific heat capacity, and emissivity of ceramic matrix composites at high temperatures, *High Temp. High Press.* 35/36 (2003) 169–177, 2004.
- [24] R. Yamada, T. Taguchi, N. Igawa, Mechanical and thermal properties of 2D and 3D SiC/SiC composites, *J. Nucl. Mater.* 283–287 (2000) 574–578.
- [25] W.X. Zhou, Y. Cheng, K.Q. Chen, G. Xie, T. Wang, G. Zhang, Thermal conductivity of amorphous materials, *Adv. Funct. Mater.* 30 (8) (2019), 1903829.
- [26] M. Verdier, K. Termentzidis, D. Lacroix, Crystalline-amorphous silicon nano-composites: nano-pores and nano-inclusions impact on the thermal conductivity, *J. Appl. Phys.* 119 (17) (2016), 175104.
- [27] D.S. Smith, A. Alzina, J. Bourret, B. Nait-Ali, F. Pennec, N. Tessier-Doyen, K. Otsu, H. Matsubara, P. Elser, U.T. Gonzenbach, Thermal conductivity of porous materials, *J. Mater. Res.* 28 (17) (2013) 2260–2272.
- [28] Y. Shi, F. Kessel, M. Friess, N. Jain, K. Tushtev, Characterization and modeling of tensile properties of continuous fiber reinforced C/C-SiC composite at high temperatures, *J. Eur. Ceram. Soc.* 41 (5) (2020) 3061–3071.
- [29] A.G. Evans, F.W. Zok, T.J. Mackin, The structural performance of ceramic matrix composites, in: S.V. Nair, J. Karl (Eds.), *High Temperature Mechanical Behaviour of Ceramic Composites*, Butterworth-Heinemann, Boston, USA, 1995, pp. 3–84.
- [30] M.Y. He, J.W. Hutchinson, Kinking of a crack out of an interface, *J. Appl. Mech.-T ASME* 56 (2) (1989) 270–278.
- [31] W.-C. Tu, F.F. Lange, A.G. Evans, Concept for a damage-tolerant ceramic composite with "strong" interfaces, *J. Am. Ceram. Soc.* 79 (2) (1996) 417–424.
- [32] D. Koch, K. Tushtev, G. Grathwohl, Ceramic fiber composites: experimental analysis and modeling of mechanical properties, *Compos. Sci. Technol.* 68 (5) (2008) 1165–1172.
- [33] E.A.V. Carelli, H. Fujita, J.Y. Yang, F.W. Zok, Effects of thermal aging on the mechanical properties of a porous-matrix ceramic composite, *J. Am. Ceram. Soc.* 85 (3) (2004) 595–602.
- [34] K. Tushtev, J. Horvath, K. Rezwani, Study on the mechanical behavior of FW12 at room and elevated temperatures, in: E.C. Walter (Ed.), *Pritzkow Spezialkeramik*, Universität Bremen Fachbereich Keramische Werkstoffe und Bauteile, Bremen, Germany, 2016.
- [35] J.A. Heathcote, X.-Y. Gong, J.Y. Yang, U. Ramamurty, F.W. Zok, In-plane mechanical properties of an all-oxide ceramic composite, *J. Am. Ceram. Soc.* 82 (10) (2004) 2721–2730.
- [36] J.C. McNulty, F.W. Zok, G.M. Genin, A.G. Evans, Notch-sensitivity of fiber-reinforced ceramic-matrix composites: effects of inelastic straining and volume-dependent strength, *J. Am. Ceram. Soc.* 82 (5) (1999) 1217–1228.
- [37] Y. Shi, S. Li, E. Sitnikova, D. Cepeli, D. Koch, Experimental evaluation and theoretical prediction of elastic properties and failure of C/C-SiC composite, *Int. J. Appl. Ceram. Technol.* (2021).
- [38] Y. Shi, N. Jain, D. Koch, Investigation and modeling of tensile failure properties of wound ceramic matrix composites, *Compos. Part A Appl. Sci. Manuf.* 114 (2018) 316–326.
- [39] Y. Shi, Y. Xiu, D. Koch, Investigation of statistical distribution of C/C-SiC composite's mechanical properties, *Key Eng. Mater.* 809 (2019) 131–139.
- [40] M. Schmücker, A. Grafmüller, H. Schneider, Mesostructure of WHIPOX all oxide CMCs, *Compos. Part A Appl. Sci. Manuf.* 34 (7) (2003) 613–622.
- [41] Y. Shi, N. Jain, R. Jemmali, S. Hofmann, D. Koch, S. Hackemann, Prediction of elastic properties for a wound oxide ceramic matrix composite material, *Int. J. Appl. Ceram. Technol.* 12 (2015) E99–E110.
- [42] G.N. Morscher, H.M. Yun, J.A. DiCarlo, In-plane cracking behavior and ultimate strength for 2D Woven and braided melt-infiltrated SiC/SiC composites tensile loaded in off-axis fiber directions, *J. Am. Ceram. Soc.* 90 (10) (2007) 3185–3193.
- [43] T. Nozawa, K. Ozawa, Y.-B. Choi, A. Kohyama, H. Tanigawa, Determination and prediction of axial/off-axial mechanical properties of SiC/SiC composites, *Fusion Eng. Des.* 87 (5–6) (2012) 803–807.
- [44] G. Camus, Modelling of the mechanical behavior and damage processes of fibrous ceramic matrix composites: application to a 2-D SiC/SiC, *Int. J. Solids Struct.* 37 (6) (2000) 919–942.
- [45] M. Steen, Tensile mastercurve of ceramic matrix composites: significance and implications for modelling, *Mater. Sci. Eng. A* 250 (2) (1998) 241–248.
- [46] M. Steen, Anomalous stress-strain behaviour of CFCCs: an extreme form of scatter, *Adv. Compos. Mater.* 8 (1) (1999) 127–134.
- [47] UBE Industries LTD, Properties of Tyranno Fiber High Temperature Type SA, 2021.
- [48] Y. Katsuda, P. Gerstel, J. Narayanan, J. Bill, F. Aldinger, Reinforcement of precursor-derived Si-C-N ceramics with carbon nanotubes, *J. Eur. Ceram. Soc.* 26 (15) (2006) 3399–3405.
- [49] O. Flores, R.K. Bordia, D. Nestler, W. Krenkel, G. Motz, Ceramic fibers based on sic and sicc systems: current research, development, and commercial status, *Adv. Eng. Mater.* 16 (6) (2014) 621–636.